


RESEARCH

Open Access



Mechanism of corrosion protection in chloride solution by an apple-based green inhibitor: experimental and theoretical studies

Mehdi Honarvar Nazari¹, Mehdi Salih Shihab², Eden Adele Havens¹ and Xianming Shi^{1*} 

Abstract

Preservation of metals in infrastructures and other assets requires cost-effective and sustainable solutions such as green corrosion inhibitors. This study assesses an apple pomace-derived green inhibitor synthesized by an innovative zero-waste method. Electrochemical measurements revealed the high performance of this liquid extract in reducing the corrosion of carbon steel in NaCl brine. The chemical composition of this inhibitor was characterized by liquid chromatography mass spectroscopy (LC-MS) to shed light on the corrosion inhibition mechanism. Based on LC-MS analysis, the results of surface analysis were interpreted. Specifically, the major corrosion inhibitor agent in the apple pomace extract was determined as C₂₆H₅₀NO₇P (1-Linoleoyl-sn-glycero-3-phosphocholine), which can adsorb onto the steel surface to form a barrier layer and serve as a blocker of active anodic sites. Further study showed that the apple extract adsorption follows the Langmuir isotherm, and physical adsorption is dominant (vs. chemical adsorption). Theoretical calculations using quantum chemistry proposed a physisorption mechanism for the protection of steel by C₂₆H₅₀NO₇P molecules.

Keywords: Green inhibitor, NaCl brine, LC-MS, Electrochemical measurements, Langmuir isotherm

Introduction

Chloride-based deicers have been used extensively in winter road maintenance operations [24, 37]. Since these chemicals are water soluble and corrosive, they can pose a great risk on the integrity, performance, and service life of steel structures (and components) [7, 43]. They may induce premature failures, which have substantial implications on the reliability, resilience, serviceability, and environmental footprints of the structure [29, 69]. One of the cost-effective methods for preventing or reducing the corrosion damage entails the application of corrosion inhibitors [20, 59, 78].

This method has been widely employed by maintenance agencies to mitigate the corrosion risk of deicers [50]. The efficiency of corrosion inhibitors is defined by their physico-chemical properties such as active functional groups, electronic structure, electron density, non-bonding (lone pair) electrons, and π -electrons [64, 66].

Traditional corrosion inhibitors contain chemical compounds that can have toxicological effects and pose harmful impacts on the receiving environment, especially surface waters [18, 30]. In recent years, green corrosion inhibitors have been introduced as alternatives to traditional inhibitors [13, 38, 40]. Bio-based materials have been used in the winter maintenance operations of roadways, either as freezing point depressant, or as green corrosion inhibitor [53]. These materials are mostly produced by

* Correspondence: xianming.shi@wsu.edu

¹Department of Civil & Environmental Engineering, Laboratory of Corrosion Science and Electrochemical Engineering, National Center for Transportation Infrastructure & Life-Extension, Washington State University, P. O. Box 642910, Pullman, WA 99164-2910, USA

Full list of author information is available at the end of the article

fermentation and processing of desugared molasses, beet juice, corn, and other agricultural products [2, 16].

Recently, the authors have introduced an innovative zero-waste method for producing agro-based corrosion inhibitors as an additive to deicer/anti-icer chemicals. The major advantage of the chemicals prepared by this method over the commercial green chemicals used by the departments of transportation (e.g., beet juice) is that the former ones feature much lower chemical oxygen demand, which makes them more eco-friendly [31]. An example of inhibitors synthesized by the innovative method is a liquid extract made from peony leaf waste, exhibiting a corrosion inhibition efficiency of 65.8% for carbon steel in NaCl brine [51]. Due to relatively low corrosion inhibition efficiency (IE) of the peony leaf extract, the authors further explored a variety of other local agro-based wastes as feedstock (such as grass, dandelion leaf, blueberry pomace, cherry pomace, and apple pomace) to produce high-efficiency “green” corrosion inhibitors. After a preliminary study, the apple pomace seemed to be the most promising agricultural waste for producing green inhibitor among the tested wastes. Therefore, we explored this feedstock further. In addition, the amount of apple waste in Washington State is 27,794 tons of dry biomass per year [27]. Therefore, the current research may lay the foundation of converting a huge amount of waste to an eco-friendly product, which can notably benefit the society and the environment.

Apple pomace has been used as a food ingredient, and for producing jam and jelly [25, 41]. Some researchers have used commercial apple-derived pectin ($C_6H_{10}O_7$) as a green inhibitor [79]. Pectin can be extracted from apple pomace using different acid extraction methods which produce solvent waste [42, 81]. However, no waste is produced during the extraction process of producing the apple pomace extract herein, which makes it a more environmentally friendly corrosion inhibitor than commercial pectin.

This work investigated the effect of an apple pomace liquid extract on the corrosion of C1010 mild steel in 3.5% NaCl brine. A zero-waste process developed by the authors was adopted to produce this “green” corrosion inhibitor. Chemical, electrochemical, and surface analyses were used to shed light on the corrosion behavior. Finally, using quantum chemical calculations we propose a mechanism of corrosion inhibition.

Experimental

Materials

The corrosion coupons were prepared from C1010 steel with a composition presented in Table 1. The exposed surface area of each coupon was 1 cm^2 . The coupons were polished by 60- to 1500-grit sandpaper sequentially, degreased by ethanol, and then washed with deionized water. In the next step, they were exposed to 3.5% NaCl brine over a 7-day period (168 h). The reason for choosing 3.5% NaCl brine for this research is that it is known that NaCl concentration of around 3% is the most corrosive concentration of NaCl brine for iron in aerated solutions at room temperature [11]. Therefore, the authors used this concentration to simulate a worst-case scenario. In the field, the concentration of 23% NaCl is the common applied concentration, for anti-icing or deicing applications. However, due to snow precipitation and ice melting conditions, the stormwater runoff tends to have much lower concentrations of NaCl.

Different concentrations of the apple pomace extract (1%, 2%, and 3% v/v (volume of extract/total volume)) were employed in this research. These values corresponded to dry mass per volume of apple pomace extract (APE) at 2.61, 5.22, and 7.82 g/L, respectively. For drying the APE, it was oven dried at 103°C for 24 h. The code names of the samples are shown in Table 2. While the range of 1–3% v/v is high relative to the range of ppm used by many researchers, it is much lower than 20% v/v that is common for using agro-based byproducts such as beet juice in winter maintenance operations. In addition, some researchers have reported the range of up to 4% v/v of alcohol-based inhibitors for protection of reinforcing steel [36].

The apple pomace extract was prepared using a chemical/biological process that has been described elsewhere in detail [51]. Briefly, in this process the apple pomace, which contained seed and peel, underwent two degradation steps: first, chemical degradation in an alkaline solution containing urea at around -13°C , then biological degradation by bacteria at room temperature. The resulting solution was heated at 85°C until its volume halved. The concentrated solution was used as the corrosion inhibitor without further treatment or purification. All the chemicals used in this research were of analytical-grade purity.

It should be mentioned that the process used in this research is more complex than the common processes of dissolving the agricultural feedstock in a solvent such as a mixture of water and alcohol, or acid [17, 76].

Table 1 Composition of the steel samples

Type of Steel	Element (wt.%)				
	C	Mn	S	P	Fe
C1010	0.08–0.13	0.30–0.60	≤ 0.05	≤ 0.04	Balance

Table 2 Code-names of the coupons in this work

Table 2. Code names of the coupons in this work				
Description	Samples exposed to 3.5% NaCl brine containing various concentrations of APE			
Inhibitor% (v/v)	0	1	2	3
Coupon code	APE0	APE1	APE2	APE3

Mass spectrometry

The liquid chromatography–mass spectrometry (LC-MS) method was employed for in-depth chemical analysis of the APE. The analysis was conducted in the positive ion mode using Synapt G2-S mass spectrometer. Calculation of the normalized weight percent (wt.%) of each compound was conducted based on the normalized percent surface area of each peak with the aid of the ImageJ software.

Electrochemical measurement

A PARSTAT MC multichannel Potentiostat performed the corrosion measurements using a standard three-electrode system comprising the working electrode (corrosion coupon), a reference electrode (Ag/AgCl, KCl saturated), and a counter electrode (platinum mesh). The electrochemical impedance spectroscopy (EIS) measurements were carried out using the same system in the frequency range of 100 kHz – 10 mHz by superimposing AC signal of ± 10 mV around the open-circuit potential (OCP). Tafel polarization test was conducted at a potential sweep rate of 0.167 mV/s in the range of -250 mV to $+250$ mV with respect to OCP. The VersaStudio software was used for running the electrochemical corrosion tests and calculating the Tafel polarization parameters, and ZSimpWin 3.60 software was employed for interpretation of the EIS data. The tests were at least duplicated to obtain an acceptable reproducibility. All of the electrochemical tests were performed at room temperature.

Surface analysis

The surface layer was examined via a JEOL JXA-8500F electron probe micro-analyzer (EPMA). The EPMA uses an electron probe to generate irradiation on the specimen surface, and then the characteristics of the produced X-ray are analyzed by wavelength-dispersive X-ray spectroscopy (WDS) techniques to qualify the element distributions on the surface. For each area, five elements (e.g. Fe, N, Cl, O, and P) were analyzed and their spatial distribution mapped.

In order to study the surface layer more in-depth, X-ray photoelectron spectroscopy (XPS) analysis was used. The analysis was carried out using an AXIS-165 multi-electron spectrometer from Kratos Analytical Inc. The data acquisition and data analysis were performed using the XPSPEAK 4.1 software.

Quantum chemical calculation

All the calculations were performed using molecular mechanics/MM+ level, and the semi-empirical calculations with PM3 method [74] at 25 °C by Hyperchem 7.52 software.

Results and discussion

Chemical composition of the liquid extract

Figure 1 and Table 3 show the results of LC-MS analysis for the APE. Based on the mass spectrum data, the APE molecules mainly include $C_{26}H_{50}NO_7P$ and $C_{31}H_{43}N_5O$ (and other organic compounds), which consist of nitrogen, oxygen, and phosphorus elements. The organic mixtures containing N, P, and O elements have polar functions, so will adsorb onto the metallic surface as

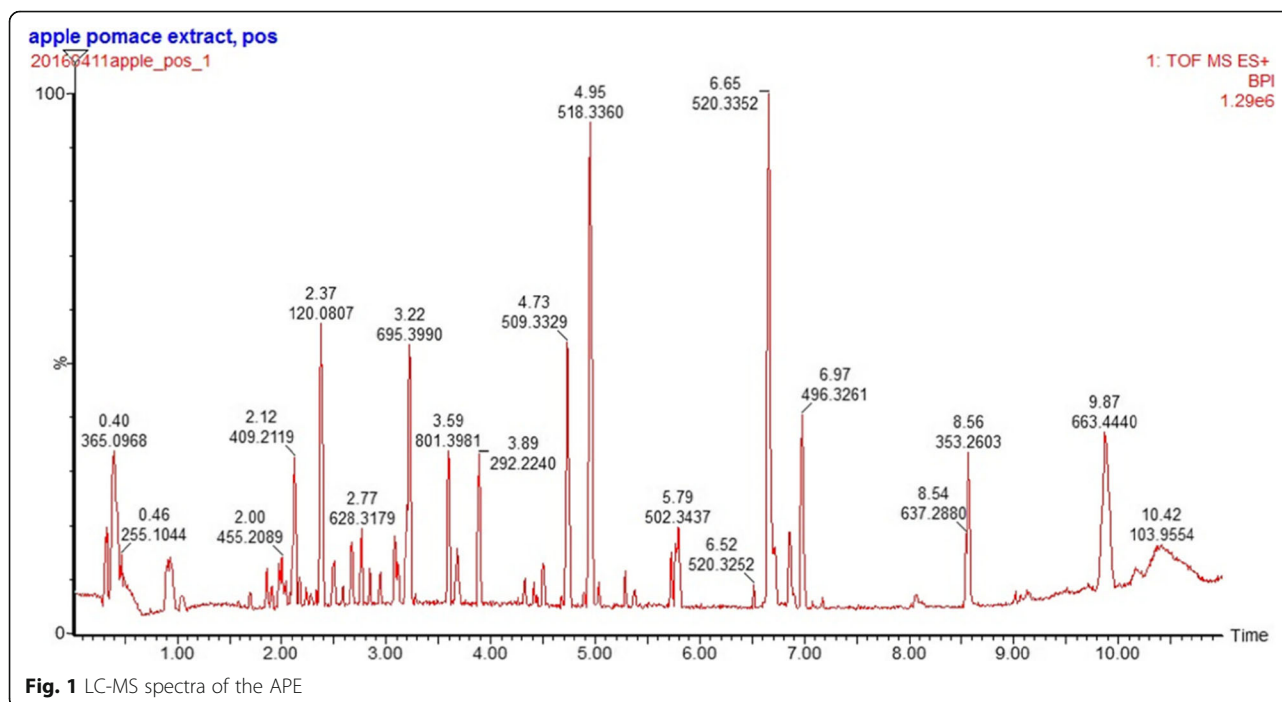


Table 3 Chemical constituents identified for APE using LC-MS analysis

Formula	Retention time (min)	m/z	wt. %
C ₁₆ H ₁₄ F ₂ N ₄ O ₄	0.40	365.0968	7.0
C ₃ H ₄ N ₂ NaO ₂ ⁺	2.37	120.0807	9.4
C ₃₂ H ₅₄ N ₈ O ₉	3.22	695.3990	10.4
C ₄₀ H ₅₄ N ₈ O ₁₁	3.59	801.3981	4.4
C ₃₁ H ₄₄ N ₂ O ₄	4.73	509.3329	7.5
C ₃₁ H ₄₃ N ₅ O	4.95	518.3360	17.3
C ₃₁ H ₄₁ N ₅ O	5.79	502.3437	3.1
C ₂₆ H ₅₀ NO ₇ P	6.65	520.3352	19.3
C ₂₇ H ₄₁ N ₇ O ₂	6.97	496.3261	7.0
C ₁₇ H ₃₂ N ₆ O ₂	8.56	353.2603	4.9
C ₄₂ H ₆₃ O ₄ P	9.87	663.4440	9.7

a barrier organic layer [19]. The adsorption of the polar atoms on the surface of metal may occur through coordination between the lone pair or π -electrons cloud and the metallic surface [23, 71].

Electrochemical characterization

OCP measurements

The OCP of steel coupons in the presence and the absence of the APE was measured after different periods of immersion in NaCl brine, as shown in Fig. 2. The OCP can be a function of corrosion potential and electrical resistivity of the protective layer formed on

the sample [83]. It can be seen that the OCPs of the samples exposed to the solutions containing the apple pomace extract shifted to more noble values, which may be a sign of the more thermodynamically steady system [33]. This conclusion has been confirmed by considering the steady trend of the OCP for sample APE3 after the third day of the experiment (72 h). This effect is not the same for all concentrations; for instance, APE2 experiences a sharp decrease in OCP values after 72 h; even more than APE1. This behavior can be due to the probabilistic nature of corrosion which causes fluctuations of OCP [28].

Tafel polarization results

Figure 3 presents the Tafel polarization plots of the samples after 7-day immersion in NaCl brines having different concentrations of APE. It is seen that addition of APE shifted the corrosion potential to a more noble potential and decreased the anodic current density. These can be ascribed to the adsorption of organic molecules on the anodic active sites of the steel surface [1, 14].

Table 4 shows the electrochemical parameters derived from the Tafel polarization plots. By increasing the concentration of the APE, the corrosion current density (i_{corr}) was notably decreased and the lowest i_{corr} was obtained at 3% (v/v) apple pomace extract. The maximum inhibition efficiency (IE%) of APE calculated using i_{corr} value was 83%, which is significantly more than that of

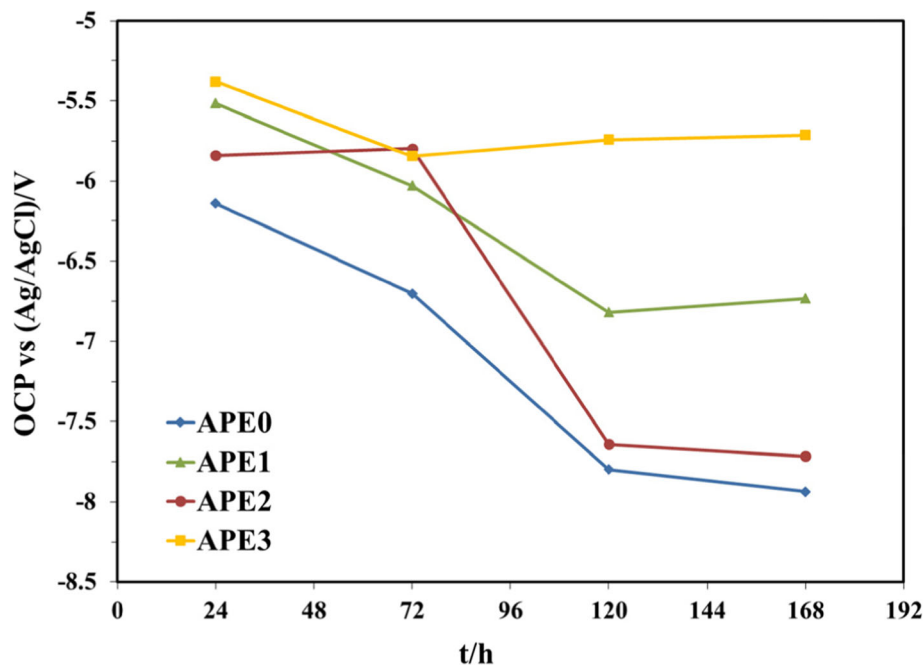


Fig. 2 OCP versus time for mild steel in NaCl brine containing 0 to 3% (v/v) APE

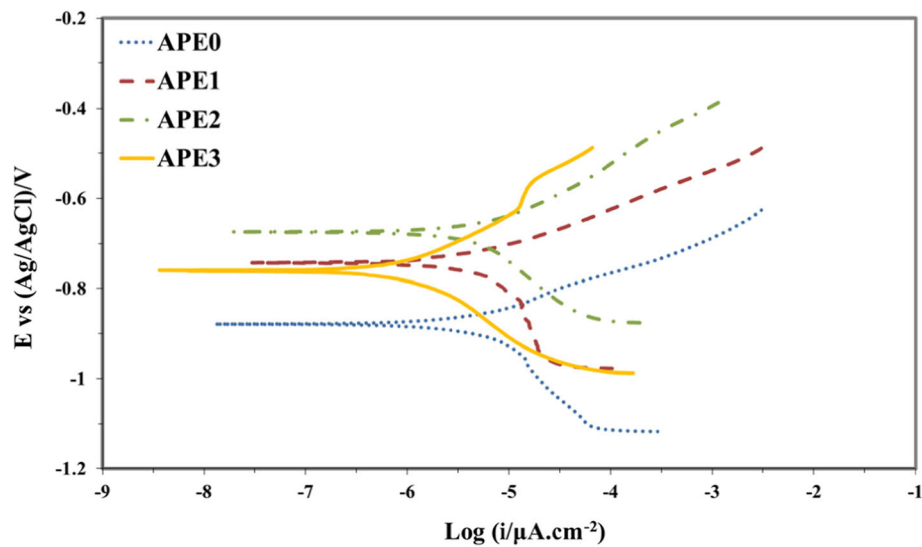


Fig. 3 Tafel polarization curves for steel samples after 7-day exposure to NaCl brine containing 0 to 3% (v/v) apple pomace extract

pectin (78.7%) for X60 steel in 0.5 M HCl solution [79] and that of Sarang Semut (*Myrmecodia Pendans*) extract (65.21%) for low carbon steel in 3.5% NaCl solution [62].

By adding the extract at 3% (v/v), the corrosion potential (E_{corr}) of the steel increased by more than 85 mV, which shows that APE is an anodic inhibitor and the corrosion inhibition is attributable to change in the activation energy [14, 21]. Based on Table 4, the values of anodic and cathodic Tafel slopes were 104.1 and 384.4 mV/dec, respectively for the APE0 sample. Both anodic and cathodic Tafel constants decreased with increases in the APE concentration.

EIS results

Figure 4 depicts the impedance Nyquist curves of steel samples in NaCl brines with various concentrations of APE. The capacitive arc radius increased by increasing the concentration of the apple pomace extract, which corresponds to improved corrosion resistance [15, 49]. The capacitive arcs for samples APE0 and APE1 have similar forms despite their different sizes, which shows that the inhibition mechanism is independent of

the extract concentration for these samples. However, the feature of the capacitive arc with a Warburg impedance emerged in samples APE2 and APE3. The observed arcs in all samples are non-ideal semi-circles which is likely due to the frequency dispersion caused by corrosion-induced non-homogeneity of the steel surface [8, 12]. In addition, adsorption of the barrier organic layer on the surface of metal can induce surface heterogeneity that can affect the shape of capacitive arc [9, 58].

The Bode curves in Fig. 5 reveal that by increasing the APE concentration, $|Z|$ value at the frequency impedance of 10 mHz ($\log f = -2$) increased. Since this value corresponds to the corrosion protection provided by the inhibitor [65], it shows that by increasing the inhibitor concentration, the corrosion protection was improved.

The equivalent electrical circuits used for studying the impedance spectra are shown in Fig. 6. The circuits consist of the following elements: R_s (solution resistance), R_f (corrosion film resistance), Q_f (constant phase element (CPE) of film), R_{ct} (charge transfer resistance of metal/solution interface), and Q_{dl} (CPE of metal/electrolyte interface), and W (Warburg impedance).

Table 4 Electrochemical parameters fitted by using Tafel polarization data

Sample Name	Tafel slopes (b/mV)		E_{corr} (mV)	i_{corr} ($\mu A/cm^2$)	IE% ^a
	β_a	$-\beta_c$			
APE0	104.1 \pm 46.7	384.4 \pm 101.1	-833.3 \pm 25.3	11.92 \pm 3.29	–
APE1	83.6 \pm 1.5	92.5 \pm 45.4	-712.2 \pm 30.5	4.60 \pm 2.24	61.4
APE2	64.8 \pm 12.0	88.6 \pm 16.7	-757.6 \pm 117.1	3.58 \pm 0.20	69.9
APE3	87.3 \pm 28.7	102.1 \pm 5.5	-728.8 \pm 31.9	2.03 \pm 1.01	83.0

Note: standard errors are reported

^aIE% = $(1 - i_{corr}(\text{inhibited}) / i_{corr}(\text{uninhibited})) \times 100$

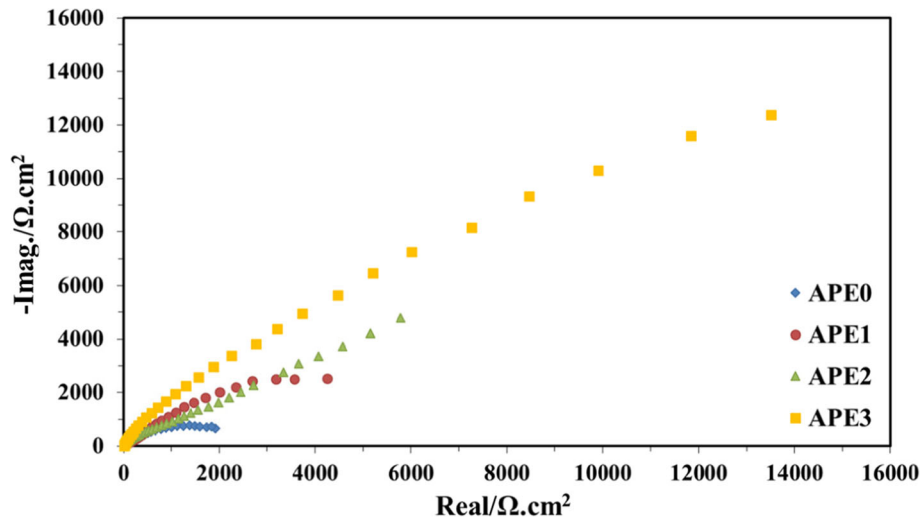


Fig. 4 Nyquist curves for steel samples after 7-day immersion in NaCl brine containing 0 to 3% (v/v) APE

Some of the values of the fitted parameters based on the equivalent electrical circuit model are summarized in Table 5. In the equivalent electrical circuit, Q_{dl} is the CPE of the electrical double layer at the metal/electrolyte interface. The CPE represents an non-ideal capacitor in the EIS results, and its impedance is stated as follows [73].

$$Z_{CPE} = \frac{1}{Y_0(j\omega)^n} \quad (1)$$

Where Y_0 is the CPE magnitude, n is the phase shift due to surface roughness ($-1 \leq n \leq 1$), and ω is the angular frequency. The values of C_{dl} , represented in Table 5, were measured as follows [44].

$$C_{dl} = (Y_0 R_{ct}^{1-n})^{1/n} \quad (2)$$

The C_{dl} values decreased with increases in the concentration of APE, which can be ascribed to the reduction of double layer dielectric constant [10]. This means a thicker electrical double layer, which is caused by more displacement of corrosive species by APE molecules at the steel/electrolyte interface [57, 75]. By increasing the concentration of APE, the values of R_{ct} increased which could translate to higher inhibition efficiencies [26]. In addition, R_f increased in the presence of higher concentrations of APE, which may pertain to the decrease in the number of ionically conducting paths. This implies a slowed-down migration rate of aggressive species (such

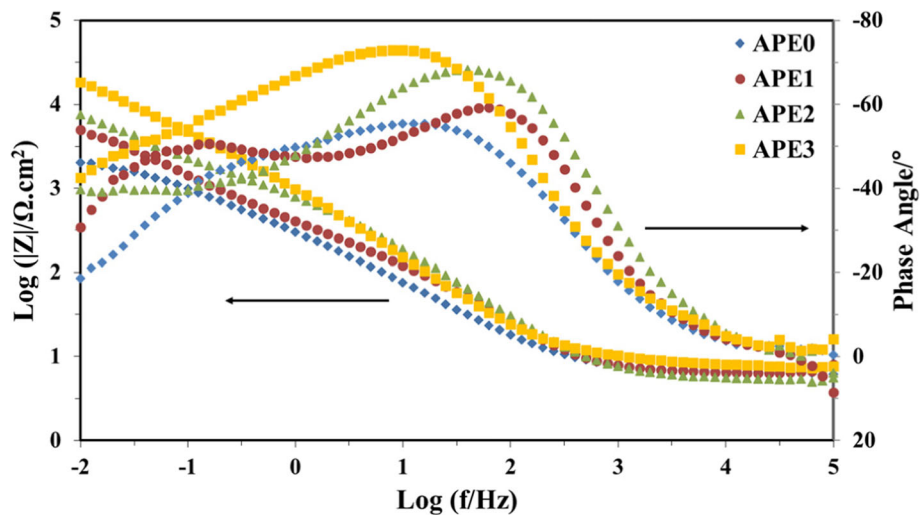


Fig. 5 Bode curves for steel samples after 7-day immersion in NaCl brine containing 0 to 3% (v/v) APE

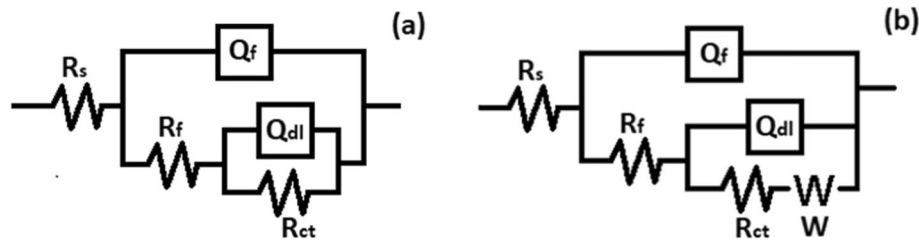


Fig. 6 Equivalent circuit models employed for assessing the EIS results

as Cl^- ions) through the adsorbed protective layer towards the surface of steel. The Warburg impedance was observed in APE2 and APE3 samples, which shows a resistance due to the diffusion process over the porosity of the corrosion product film [32, 35].

The fitted curves for Nyquist and Bode curves of samples APE0 and APE3 are shown in Fig. 7. As can be seen, there is a good match between the modeled and experimental results. For modeling the electrochemical behavior of samples APE0 and APE3, the equivalent circuits presented in Fig. 6 (a) and 6 (b) were used, respectively. The maximum IE of APE calculated using EIS data was 98.8%, which was much more than that of pectin (77.1%) for X60 steel in 0.5 M HCl solution [79] and that of Myrmecodia Pendans extract (79.7%) for the corrosion of mild steel API 5 L Grade B in 3.5% NaCl [63].

The Nyquist curves of the APE3 sample at various immersion periods are shown in Fig. 8. The protection responses were modified over time, controlled by the charge transfer mechanism for all time periods. The biggest capacitance arc was observed at day 7, which showed the stability of the protective layer over time. The Bode curves depicted in Fig. 9 demonstrate the increasing of the $|Z|_{10\text{mHz}}$ with APE concentration, which shows improvement in anti-corrosion performance of the inhibitor and its stability over time. After five days of immersion, the Bode curve showed the fingerprint of two time constants, which can be explained by the

changing of the protection mechanism from geometry blocking to energy effect [14]. This is in good agreement with Tafel results that linked the APE corrosion inhibition to changing of the activation energy.

Adsorption isotherm

The interaction of APE molecules with the steel surface can be determined by using an adsorption isotherm. In this regard, the surface coverage degree (θ) was assumed to be equivalent to inhibition efficiency (IE) measured by the EIS technique. The IE versus APE concentration was fitted to Langmuir, Freundlich, Flory-Huggins, and Temkin adsorption isotherms. The Langmuir isotherm exhibited the best fit to the data, with the correlation coefficient of 0.997 (Fig. 10). The Langmuir isotherm follows the following equation [54].

$$\log\left(\frac{C}{\theta}\right) = \log C - \log K \quad (3)$$

Where C is the concentration of APE in g/L (dry mass/volume of extract solution), K is the adsorption coefficient (L/g). Classical adsorption isotherms (such as Langmuir) use the model of non-penetrable interface in which a solvent can be substituted by the molecules of an adsorbate [45].

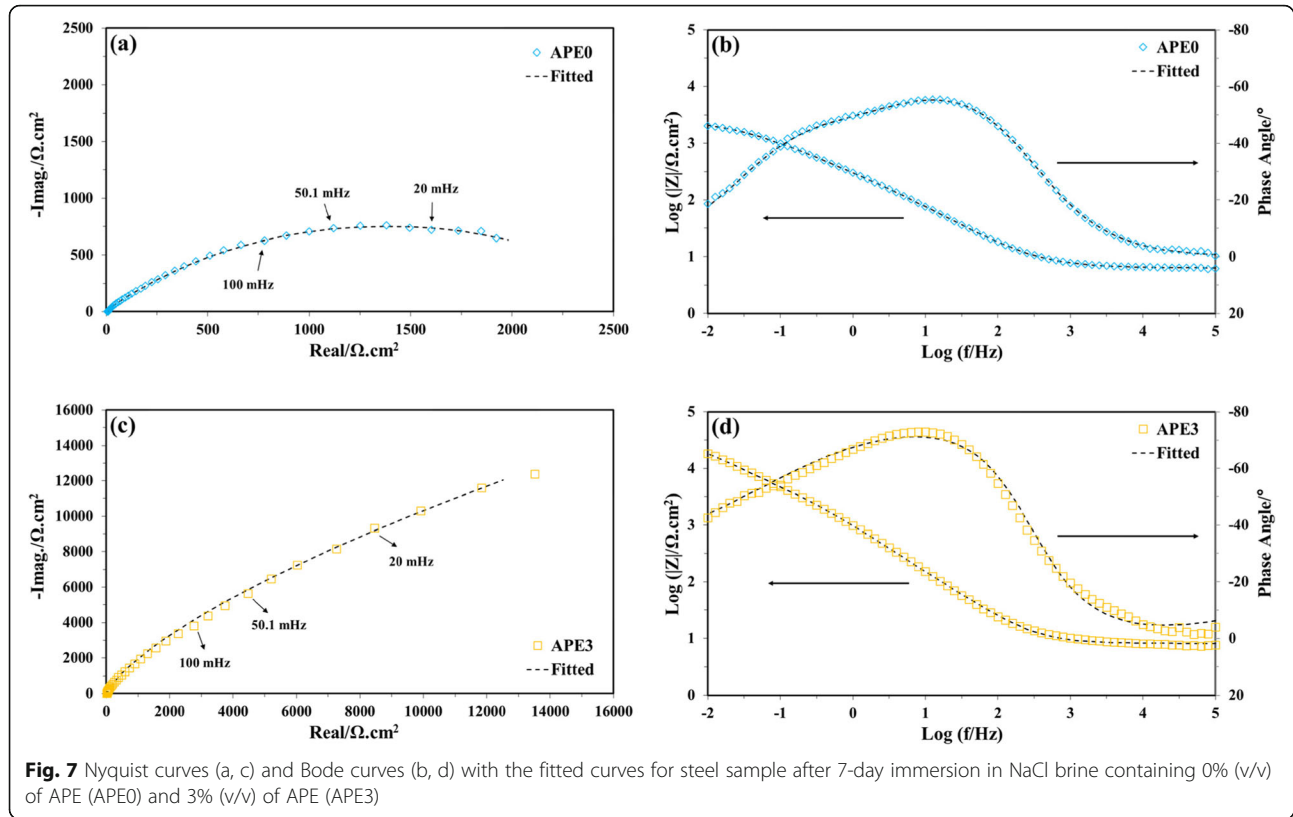
Table 5 EIS parameters obtained by fitting the data to an equivalent circuit for the samples immersed for 7 days in NaCl brine

Sample Name	R_f ($\Omega \text{ cm}^2$) $\times 10^2$	$\frac{Q_f}{Y_{of}}$ ($\Omega^{-1} \text{ cm}^{-2} \text{ s}^{n_f}$) $\times 10^{-4}$	n_f	C_f (F cm^{-2}) $\times 10^{-4}$	R_{ct} ($\text{K}\Omega \text{ cm}^2$)	$\frac{Q_{dl}}{Y_{odl}}$ ($\Omega^{-1} \text{ cm}^{-2} \text{ s}^{n_{dl}}$) $\times 10^{-4}$	n_{dl}	C_{dl} (F cm^{-2}) $\times 10^{-4}$	W ($\Omega \text{ cm}^2 \text{ s}^{-1/2}$)	R_p^a ($\text{K}\Omega \text{ cm}^2$)	IE% ^b
WAPE0	1.48 \pm 1.17	18.69 \pm 8.00	0.64 \pm 0.10	4.76 \pm 3.27	1.09 \pm 0.04	7.61 \pm 3.51	0.83 \pm 0.11	7.48 \pm 3.73	–	1.24	–
WAPE1	1.42 \pm 0.68	2.99 \pm 1.25	0.62 \pm 0.23	0.63 \pm 0.32	7.67 \pm 1.08	12.08 \pm 3.84	0.66 \pm 0.10	95.59 \pm 77.55	–	7.82	84.2
WAPE2	5.78 \pm 2.72	2.10 \pm 0.76	0.83 \pm 0.01	1.02 \pm 1.33	10.56 \pm 7.46	5.99 \pm 1.43	0.61 \pm 0.04	23.63 \pm 19.87	75.75 \pm 75.74	11.13	88.9
WAPE3	3.39 \pm 3.35	3.26 \pm 1.71	0.47 \pm 0.19	0.44 \pm 0.44	99.28 \pm 98.31	3.28 \pm 1.89	0.82 \pm 0.03	3.04 \pm 1.27	1.02 \pm 1.01	99.61	98.8

Note: standard errors are reported

^a $R_p = R_f + R_{ct}$

^bIE% = $(1 - R_p(\text{uninhibited}) / R_p(\text{inhibited})) \times 100$

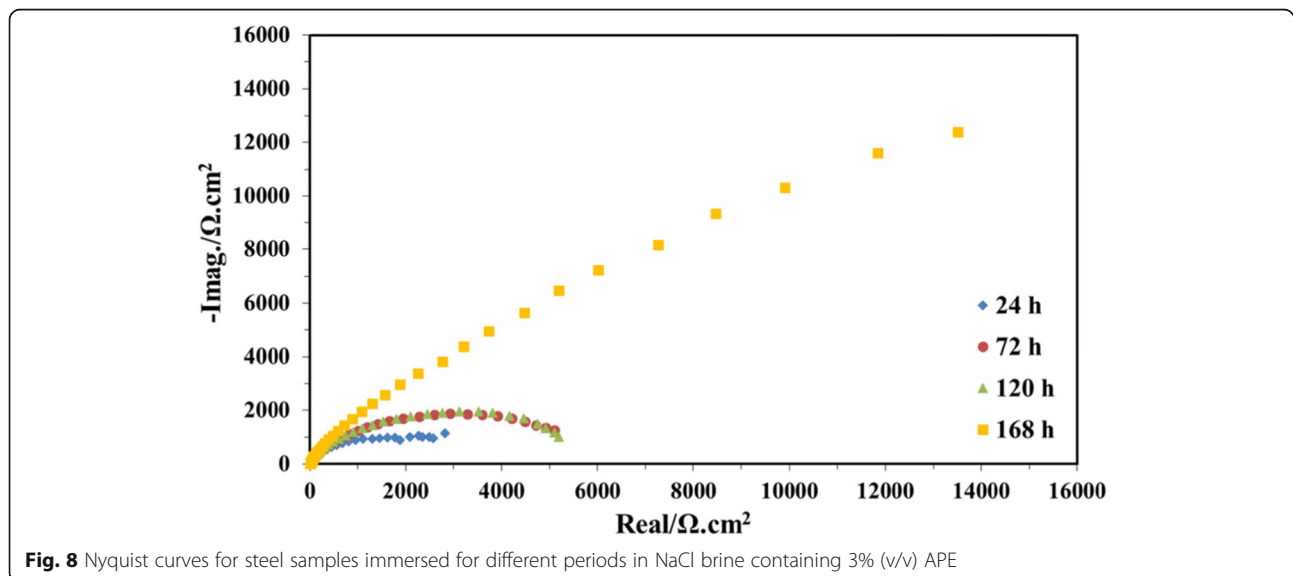


The change in the free energy of adsorption (ΔG_{ads}^0) was measured as follows [54, 68].

$$\Delta G_{ads}^0 = -2.303RT \log(C_{solvent}K) \quad (4)$$

Where R designates the gas constant, T shows the absolute temperature, K is the adsorption coefficient (L/g), and $C_{solvent}$ is the water concentration (1000 g/L). The

Gibbs free energy was estimated to be $-16.33 \text{ kJ mol}^{-1}$. The negative value of ΔG_{ads}^0 suggested the spontaneous occurrence of adsorption process of APE species onto the steel surface. The absolute value of Gibbs free energy was smaller than 20 kJ mol^{-1} , which suggests that the physical adsorption is dominant, rather than chemical adsorption [72]. In this condition, the electronic structure of the adsorbate is disturbed because of the



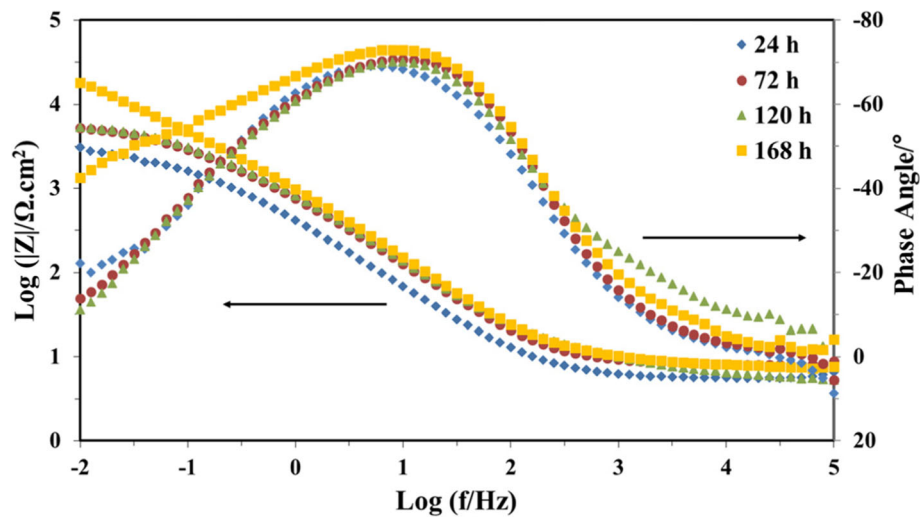


Fig. 9 Bode curves for steel samples immersed for different periods in NaCl brine containing 3% (v/v) APE

electrostatic interaction between APE molecules and the steel surface [70].

Surface analyses

SEM micrographs

The SEM images of as-washed coupons are provided in Fig. 11. A rough surface was observed on the uninhibited sample (APE0) and smoother surfaces on the samples exposed to APE containing solutions. Other researchers for the uninhibited and inhibited samples in Cl^- containing media reported similar results [3]. The amount of

metallic surface covered by the organic layer increased with increases in the concentration of APE. This is in good agreement with the results obtained by electrochemical measurements and adsorption isotherm.

EDS results

The main elements of the surface layer formed on the as-washed APE0 – APE3 steel samples are shown in Fig. 12. The main peaks for all samples corresponded to iron and oxygen, which suggests the formation of iron oxides on the surface. This is in good agreement with the results

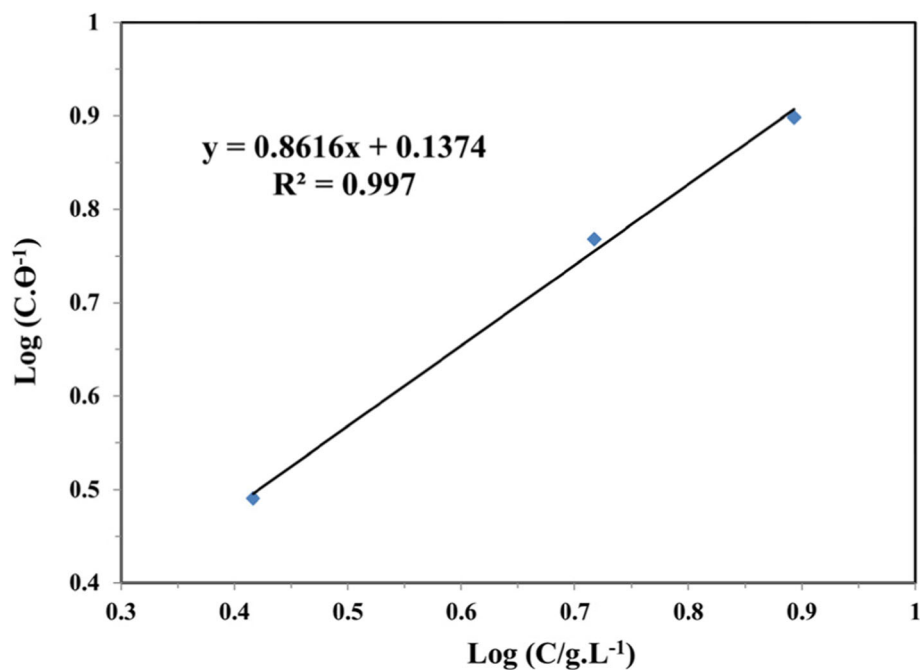


Fig. 10 The isotherm for adsorption isotherm of APE (C, in g/L, dry mass per volume of corresponding APE)

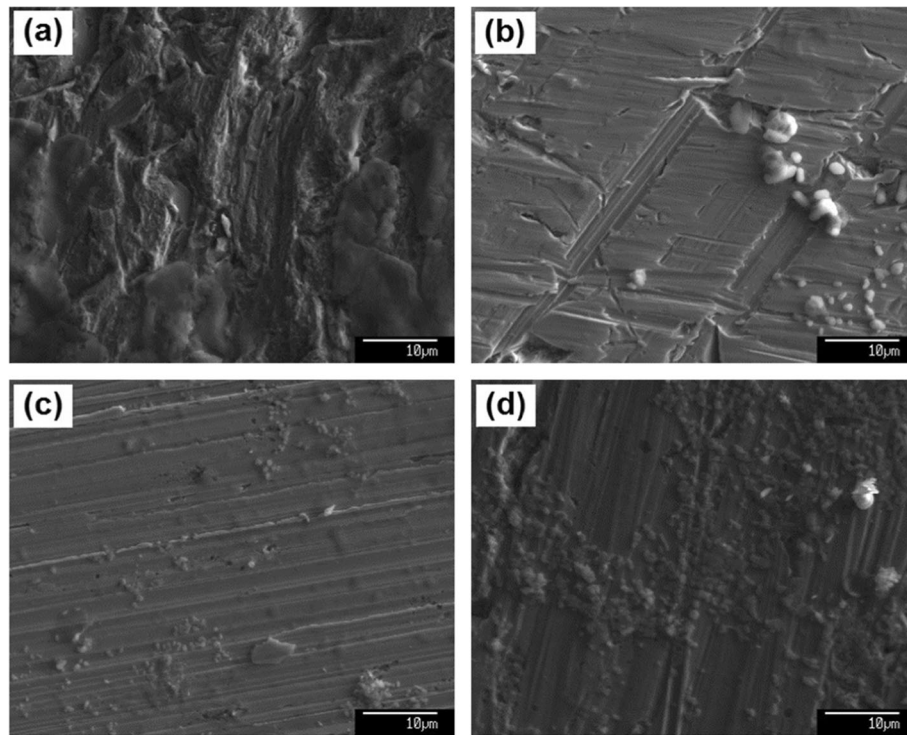


Fig. 11 SEM micrographs of as-washed coupons after 7-day immersion in NaCl brine with APE at (a) 0%, (b) 1%, (c) 2%, and (d) 3% (v/v)

obtained by EIS measurement that suggested the formation of a corrosion product layer on the surface of steel. In the case of APE3, a relatively large peak related to phosphorus can be seen around 2 keV, which is attributed to the adsorption of inhibitor molecules onto the steel surface.

EPMA results

For more in-depth analysis of the corrosion surface layer, EPMA analysis was employed which enables simultaneous detection of different elements and mapping of their distribution on a defined surface area. The EPMA elemental maps for the surface

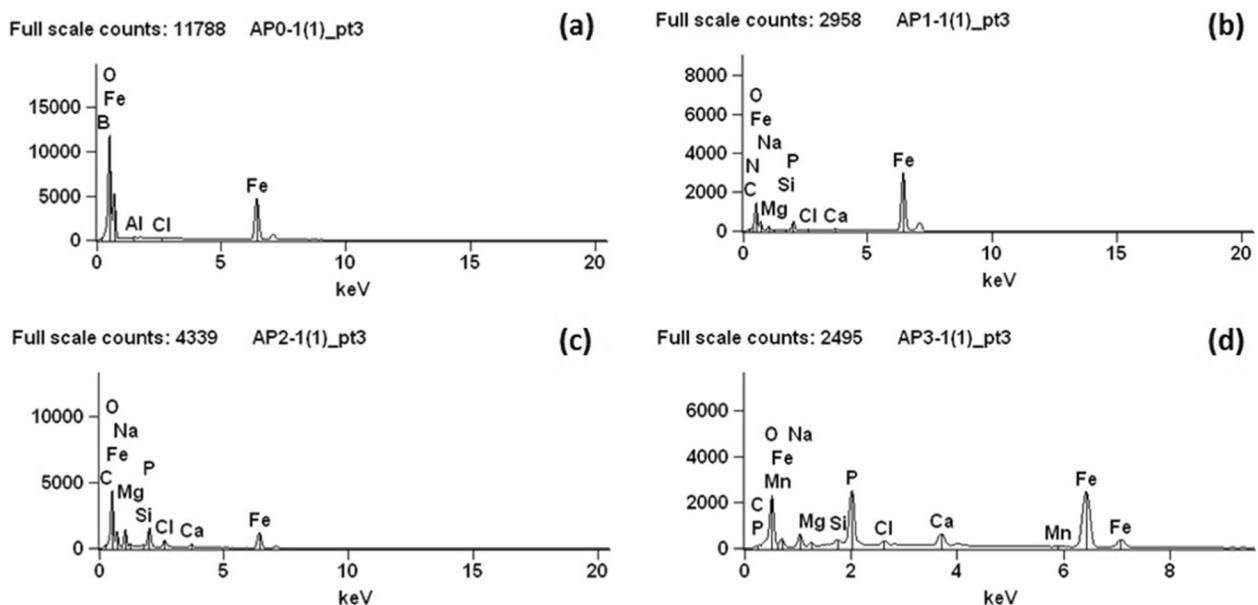


Fig. 12 EDS results of the corrosion surface layer for (a) APE0, (b) APE1, (c) APE2, (d) APE3 steel samples

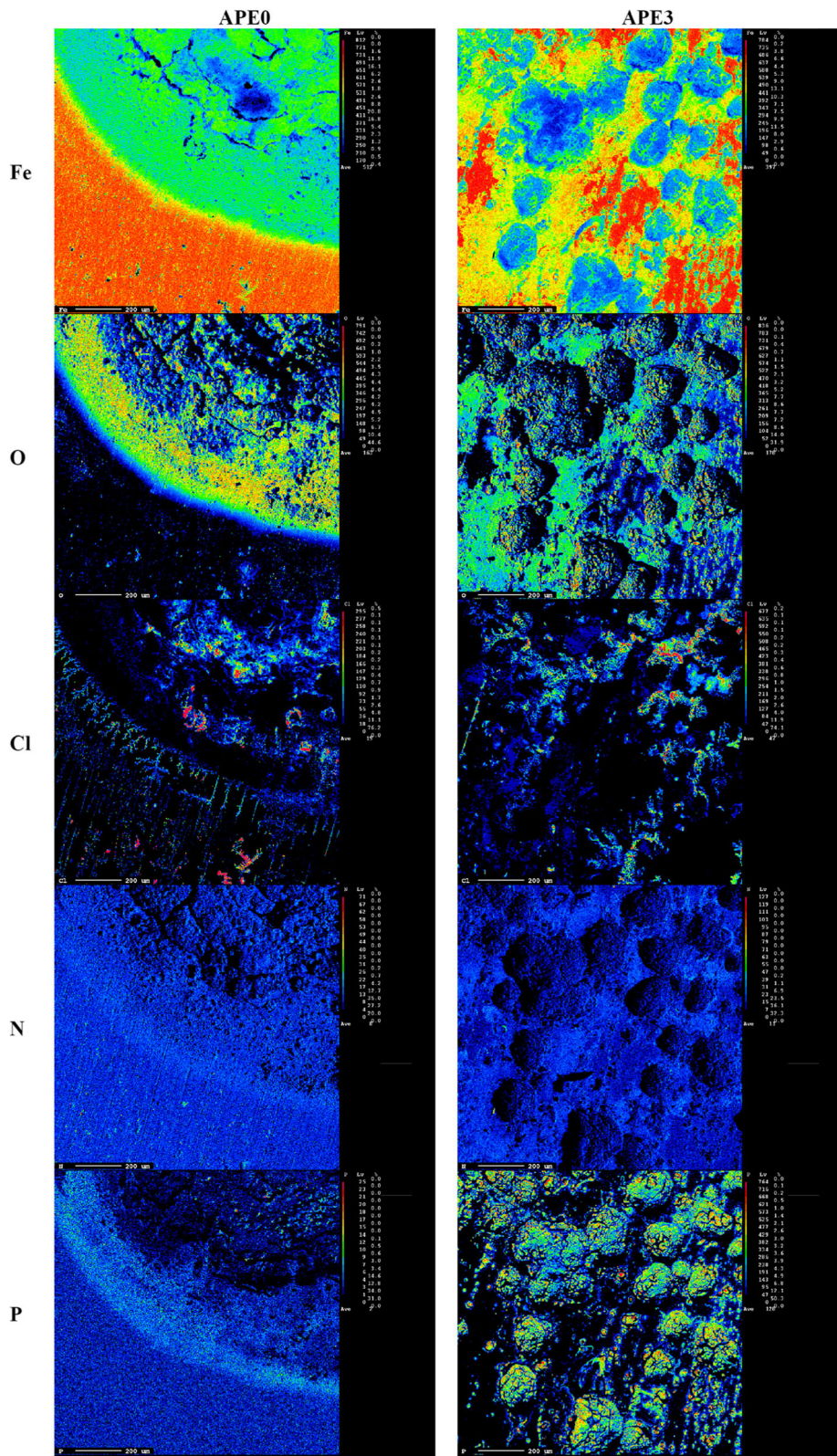


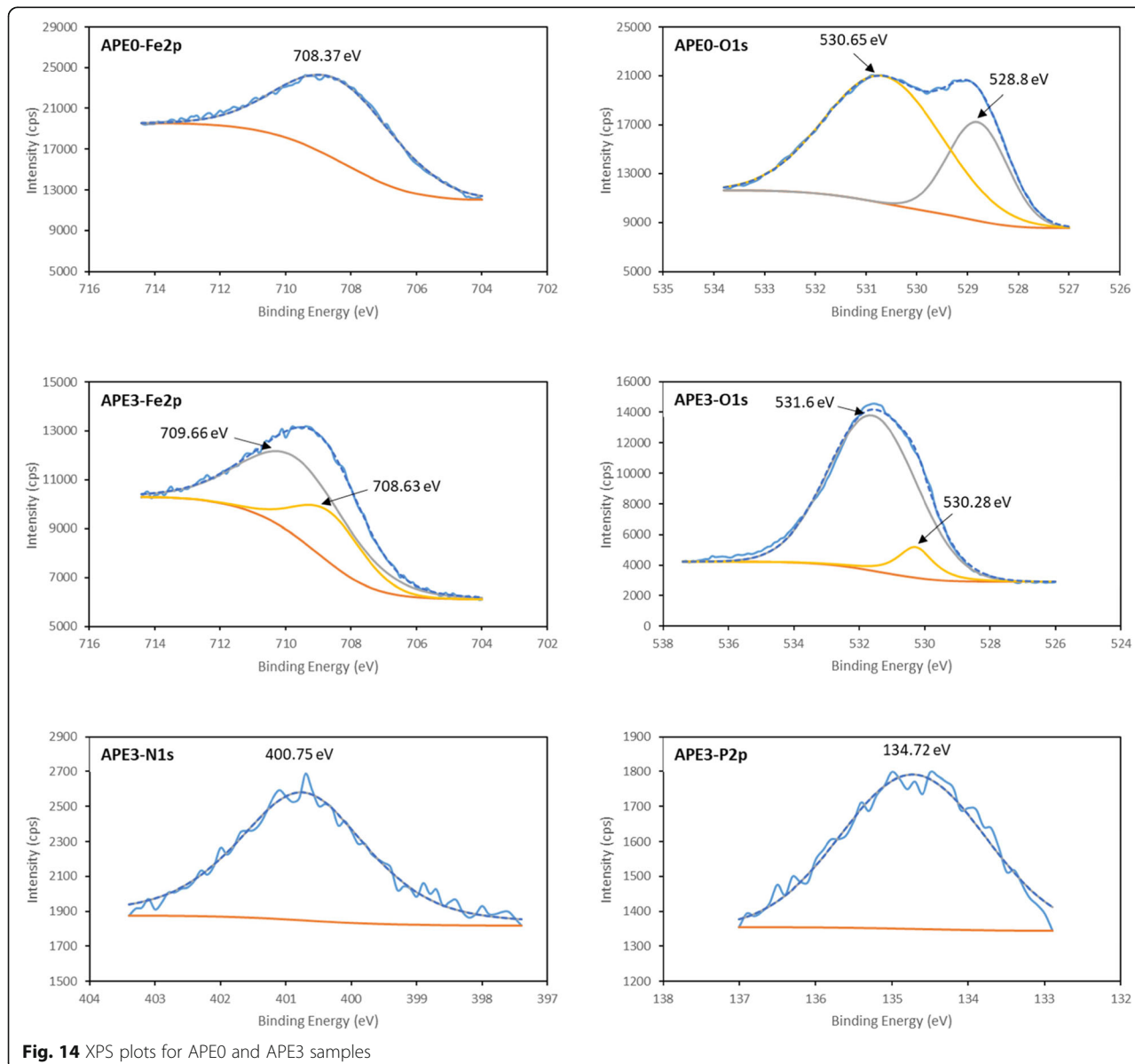
Fig. 13 EPMA maps of the corrosion surface layer for APE0 and APE3 steel samples. The size of analyzed area was set at 50 μm × 50 μm

layer formed on the APE0 and APE3 steel samples are shown in Fig. 13. On the steel surface exposed to uninhibited NaCl brine (APE0), there is little presence of N or P and the corrosion product layer consisted of an iron oxide/hydroxide layer containing Cl. The interface between the corroded surface (left) and the intact steel substrate (right) is clearly illustrated by the elemental maps of Fe, O and Cl. In contrast, the surface layer in NaCl brine with high inhibitor concentration (APE at 3%) clearly consisted of a phosphorous compound. These results are in very good agreement with the results obtained by EDS. Therefore, from these results and the LC-MS data it can be concluded that $C_{26}H_{50}NO_7P$ is the major corrosion

inhibitor agent in the APE. The charge density of phosphates is more negative than that of amines [34]; as such, the bond of former with metallic surface is more stable.

XPS results

Figure 14 depicts the results of XPS analysis for WPE0 and WPE3 samples. In the plot associated with Fe2p in WPE0, there is a peak at 708.37 eV which is related to Fe_3O_4 [46]. The XPS analysis of O1s unveils two peaks at 530.65 eV and 528.8 eV, which are associated with Fe_3O_4 and Fe_2O_3 complexes, respectively [4, 5]. In the presence of APE (sample APE3), two peaks appeared in the Fe2p plot. The major peak seen at 709.66 eV comes from Fe_2O_3 [60]. The second peak at 708.63 is due to



Fe_3O_4 [46]. Therefore, in the presence of APE, the major part of corrosion product layer is converted to Fe_2O_3 from Fe_3O_4 . It is known that Fe_2O_3 is more corrosion-resistant than Fe_3O_4 [39]. As such, one of the reasons that APE3 has a less corrosion rate than APE0 is the catalytic effect of APE in converting Fe_3O_4 to Fe_2O_3 in corrosion surface layer. It is known that phosphates can catalyze the oxygen evolution at near neutral pH [77]. In addition, they can stabilize the corrosion product layer [47]. Therefore, $\text{C}_{26}\text{H}_{50}\text{NO}_7\text{P}$ played the main role in converting Fe_3O_4 to Fe_2O_3 . Observation of the N1s plot shows a peak at 400.75 eV that indicates adsorption of an amine-containing compound on the steel surface [82], which may be $\text{C}_{31}\text{H}_{43}\text{N}_5\text{O}$. In addition, the plot of P2p shows a peak at 134.72 eV that reveals an amine-phosphate based constituent [61], which may have resulted from the adsorption of $\text{C}_{26}\text{H}_{50}\text{NO}_7\text{P}$ compound.

Quantum chemical calculations

Theoretical studies have prospective applications in designing and developing of many organic inhibitors in the field of corrosion inhibition chemistry. The capability of the inhibitor for corrosion prevention bases on its spatial distribution of molecule and its electronic arrangement over frontier molecular orbitals. Molecular geometry systems of compounds $\text{C}_{26}\text{H}_{50}\text{NO}_7\text{P}$ and $\text{C}_{31}\text{H}_{43}\text{N}_5\text{O}$ as the main compounds of the APE were determined. The stable geometry of the compounds was obtained by PM3 method, which was carried out in Hyperchem software (Fig. 15).

The calculated chemical parameters for $\text{C}_{26}\text{H}_{50}\text{NO}_7\text{P}$ and $\text{C}_{31}\text{H}_{43}\text{N}_5\text{O}$ molecules are given in Table 6. It is seen that the dipole moments (μ) for $\text{C}_{26}\text{H}_{50}\text{NO}_7\text{P}$ and $\text{C}_{31}\text{H}_{43}\text{N}_5\text{O}$ molecules are 17.0 D and 6.6 D, respectively. The organic molecules with high dipole moment may

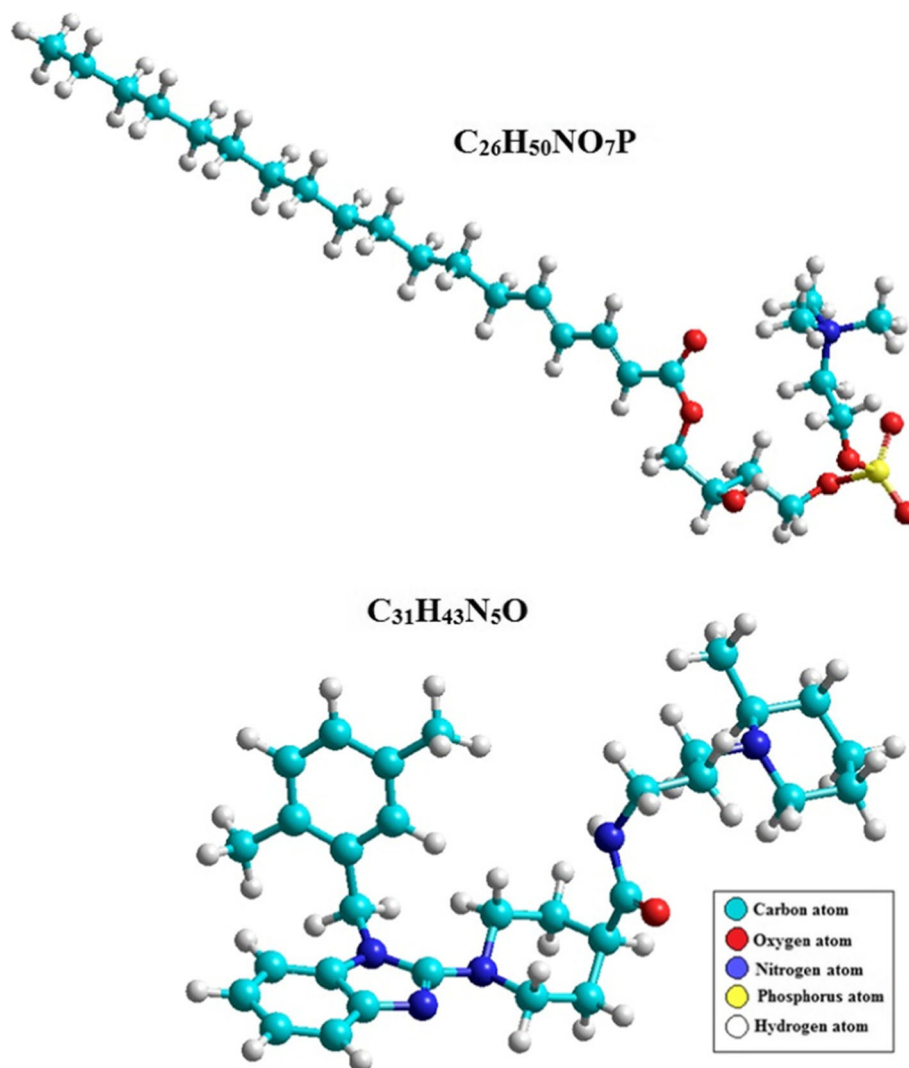


Fig. 15 Conformation structure for $\text{C}_{26}\text{H}_{50}\text{NO}_7\text{P}$ and $\text{C}_{31}\text{H}_{43}\text{N}_5\text{O}$

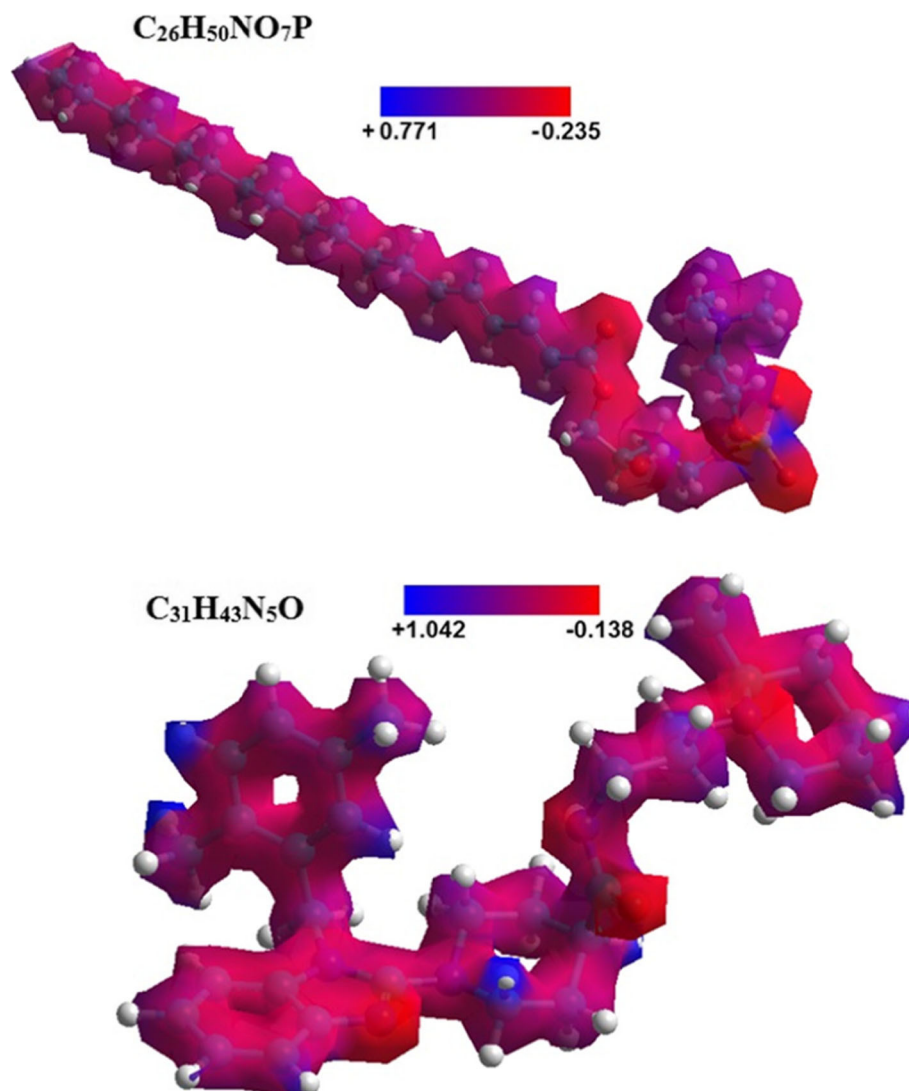
Table 6 Quantum calculation results of the APE obtained by using PM3 method

Molecule	E_{HOMO} (eV)	E_{LUMO} (eV)	Energy gap (ΔE , eV)	μ (Debye)
$\text{C}_{26}\text{H}_{50}\text{NO}_7\text{P}$	-8.863	-1.108	7.755	17.0
$\text{C}_{31}\text{H}_{43}\text{N}_5\text{O}$	-8.471	-0.093	8.378	6.6

form electrostatic interactions with the metal surface, that result in a strong adsorption on the surface of metal [55]. In this research, the value of μ for $\text{C}_{26}\text{H}_{50}\text{NO}_7\text{P}$ is more than twice of the value of μ associated with $\text{C}_{31}\text{H}_{43}\text{N}_5\text{O}$. This can justify the better corrosion inhibition properties of $\text{C}_{26}\text{H}_{50}\text{NO}_7\text{P}$ relative to $\text{C}_{31}\text{H}_{43}\text{N}_5\text{O}$. These results are also in good agreement with the results obtained by Verma et al. that showed D-glucose derivatives with the dipole moment of 8.17 D having more than 96% corrosion inhibition efficiency in 1 M HCl

solution [80]. In addition, the μ value of $\text{C}_{26}\text{H}_{50}\text{NO}_7\text{P}$ (17.0 D) is more than that of pectin, 11.725 D [79], which justifies the better anti-corrosion performance of APE than pectin.

The energy gap ($\Delta E = E_{\text{LUMO}} - E_{\text{HOMO}}$) between the E_{LUMO} and E_{HOMO} levels of inhibitor molecules is another important electronic parameter which is given in Table 6. The values of energy gap for $\text{C}_{26}\text{H}_{50}\text{NO}_7\text{P}$ and $\text{C}_{31}\text{H}_{43}\text{N}_5\text{O}$ molecules are 7.7548 eV and 8.3776 eV, respectively. Low absolute values of the energy gap means good inhibition efficiency of the organic inhibitor [56]. It is evident that $\text{C}_{26}\text{H}_{50}\text{NO}_7\text{P}$ has a lower energy gap than $\text{C}_{31}\text{H}_{43}\text{N}_5\text{O}$. This confirms the EDS and EPMA results, which showed that $\text{C}_{26}\text{H}_{50}\text{NO}_7\text{P}$ is the main corrosion inhibitor agent in the APE. Similar observations have been reported by Aloysius et al. where VB7 with the ΔE of 3.769 eV showed stronger affinity towards the steel

**Fig. 16** Electrostatic potential maps of $\text{C}_{26}\text{H}_{50}\text{NO}_7\text{P}$ and $\text{C}_{31}\text{H}_{43}\text{N}_5\text{O}$

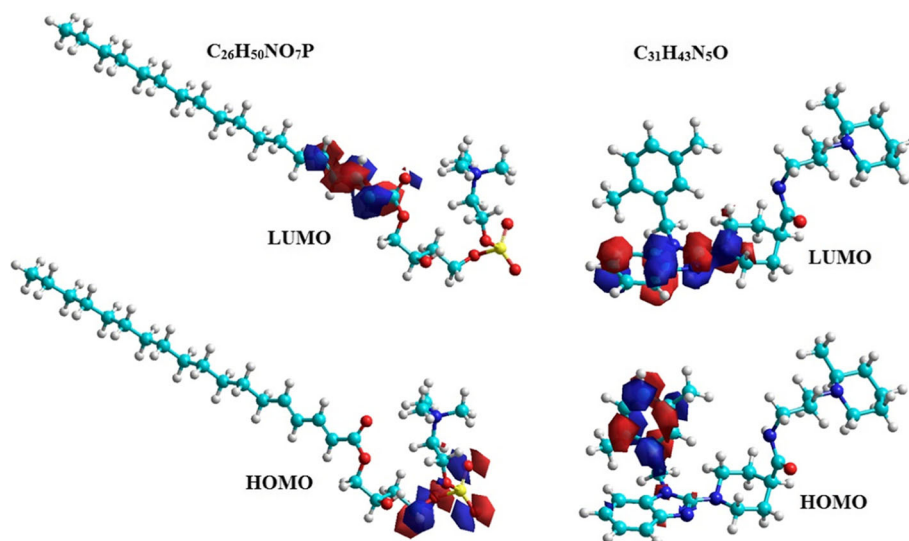


Fig. 17 LUMO and HOMO distributions for $C_{26}H_{50}NO_7P$ and $C_{31}H_{43}N_5O$

surface and better inhibition efficiency than VB1 with the ΔE of 6.555 eV [6].

Figure 16 displays the electrostatic potential maps for $C_{26}H_{50}NO_7P$ and $C_{31}H_{43}N_5O$ molecules. More dark red (negative) regions associated with nucleophilic reactivity in the potential map of $C_{26}H_{50}NO_7P$ and $C_{31}H_{43}N_5O$ indicate that these molecules are readily sharing free electron pairs with the metal surface (electrophilic agent) through electrostatic interactions. Also, the molecules with blue (positive) region have electrophilic reactivity [22].

Figure 17 displays the frontier orbitals including the highest occupied molecular orbital (HOMO) and the lowest unoccupied molecular orbital (LUMO) for $C_{26}H_{50}NO_7P$ and $C_{31}H_{43}N_5O$ molecules. It can be seen in the HOMO of $C_{26}H_{50}NO_7P$ molecule that the isosurfaces have been localized via phosphate moiety. This moiety has donor sites that facilitate the adsorption on the

metallic surface by O atoms. However, the side chain (trimethyl amine and ester group) did not contribute to the HOMO electronic distribution. On the other hand, LUMO of $C_{26}H_{50}NO_7P$ molecule plays the role of acceptor where the electronic distribution is localized on the O atoms of ester moiety and C atoms of C=C bonds. In addition, O atoms of phosphate moiety are able to coordinate with positive ions of the surrounding environment.

In Fig. 17, it can be seen that HOMO isosurfaces are localized in $C_{31}H_{43}N_5O$ via benzoimidazole and piperidine moieties. Benzoimidazole and piperidine moieties have donor sites of $C_{31}H_{43}N_5O$ that facilitate the adsorption on the metallic surface by N atoms. Nevertheless, the side chain (aryl groups and amide) has not any influence on the electronic distribution of the HOMO in $C_{31}H_{43}N_5O$. In addition, N atoms of benzoimidazole and piperidine moieties have active sites to coordinate with ions, which enables them to be acceptor of electron. Finally, the

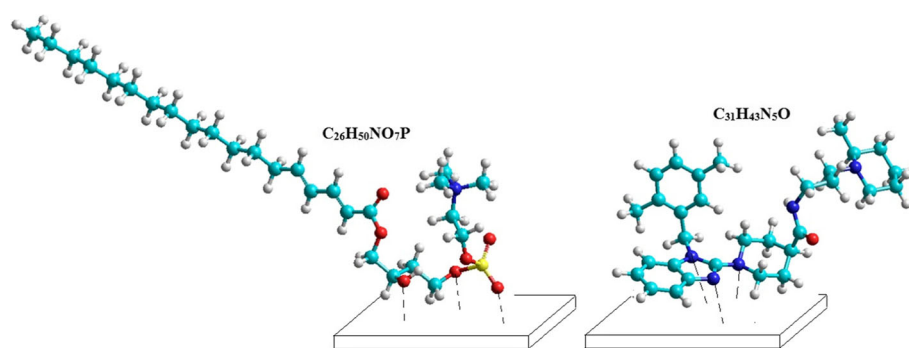


Fig. 18 Physisorption mechanism of $C_{26}H_{50}NO_7P$ and $C_{31}H_{43}N_5O$ molecules on the steel surface

theoretical studies revealed that the hydrocarbon groups attached to $C_{26}H_{50}NO_7P$ and $C_{31}H_{43}N_5O$ have no effect on LUMO or HOMO distributions and can just be as hydrophobic fragments.

It was observed that nitrogen and oxygen atoms in the studied molecules have high electron density. These sites are nominated to be the active sites to proper electrophiles and can be attached within the environment [48]. Based on this, a physisorption mechanism was proposed for adsorption of $C_{26}H_{50}NO_7P$ and $C_{31}H_{43}N_5O$ molecules on the metallic surface, as depicted in Fig. 18.

Mechanism of corrosion inhibition

The inhibition mechanism in the presence of APE was adsorption of an organic protective film, and chemical conversion of corrosion product layer to a more corrosion-resistant film. The adsorption type was Langmuir isotherm model in which a monolayer of organic molecules form a non-penetrable interface. In the Langmuir model, each active site on the metal surface can be related equally to an adsorbate molecule, and there is no interaction among the adsorbed molecules [67]. In addition, the saturation coverage occurs when all of the surface active sites are occupied by the adsorbate molecules [67]. According to the experimental results, the saturation behavior in the inhibitive characteristics occurred in 3% v/v of APE in this research, since the corrosion efficiency at this concentration of APE is close to 100%, thus it cannot increase considerably.

1-Linoleoyl-sn-glycero-3-phosphocholine ($C_{26}H_{50}NO_7P$) has a major role in the inhibition properties of APE. The corrosion inhibitive behavior of $C_{26}H_{50}NO_7P$ can be related to the functional group of its molecular structure [52]. It was also responsible for converting Fe_3O_4 in corrosion product layer to a more corrosion-resistant iron oxide (Fe_2O_3). APE molecules may attach to the surface of steel through their high electron density sites [70]. The APE adsorption entails the interaction of non-bonding electrons on nitrogen and oxygen with the steel surface.

More APE was associated with higher R_{ct} and R_f values which shows the formation of a more protective surface layer. On the other hand, more APE corresponded to lower values of C_{dl} , due to displacement of corrosive agents by organic molecules via an adsorption process at the metal/media interface. The inhibition efficiency was improved by increasing of APE concentration, which indicates an active corrosion protection. The corrosion protection mechanism changed over time from geometry blocking to energy effect. APE molecules blocked the anodic active sites and shifted the corrosion potential to more passive values. The amount of this shift was more than 85 mV, and this suggests that APE is an anodic inhibitor and inhibition property is due to the change of activation energy.

Conclusions

This research assessed the corrosion behavior of C1010 steel in 3.5% NaCl brine in the presence of an apple pomace liquid extract. The corrosion mechanism in the presence of this extract was elucidated using electrochemical measurements, mass spectroscopy, and surface analyses and the following key findings have been obtained.

- Apple pomace extract acted as a “green” corrosion inhibitor. The inhibition efficiency increased with increasing the concentration of the extract and over time.
- An excellent inhibition efficiency of 98.8% was achieved at 3% of this green inhibitor after 7-day of immersion in NaCl media.
- Apple pomace extract molecules adsorbed onto the surface of steel following the Langmuir isotherm and physical adsorption was dominant (vs. chemical adsorption).
- The apple pomace extract blocked anodic active sites on the surface of steel, and converted Fe_3O_4 to Fe_2O_3 , which is a more corrosion-resistant iron oxide.
- The main corrosion inhibitor agent in the apple pomace extract was $C_{26}H_{50}NO_7P$ molecule.
- The protection mechanism improved over time from geometry blocking to energy effect.
- The quantum chemical calculations confirm the experimental results and suggest the physisorption mechanism of this green corrosion inhibitor.

Abbreviations

LC-MS: Liquid chromatography mass spectroscopy; IE: Inhibition efficiency; APE: Apple pomace extract; v/v: Volume of extract/total volume; wt.: Weight; EIS: Electrochemical impedance spectroscopy; OCP: Open-circuit potential; μ : Dipole moments; EPMA: Electron probe micro-analyzer; WDS: Wavelength-dispersive X-ray spectroscopy; XPS: X-ray photoelectron spectroscopy; i_{corr} : Corrosion current density; E_{corr} : Corrosion potential; W: Warburg impedance; θ : Surface coverage degree; ΔG_{ads}^0 : Free energy of adsorption; ΔE : Energy gap; HOMO: Highest occupied molecular orbital; LOMO: Lowest unoccupied molecular orbital

Acknowledgments

The authors would like to acknowledge Dr. Girish Ganjyal (School of Food Science, Washington State University) for providing the apple pomace powder.

Authors' contributions

Dr. M. Honarvar Nazari did final interpretation of the results of the electrochemical corrosion tests, conducted some of the laboratory tests and wrote the draft manuscript. Dr. M. S. Shihab conducted the quantum chemical calculations, provided the quantum chemical figures, and wrote an initial draft of the related section. E. A. Havens conducted most of the electrochemical tests and did an initial interpretation on the related data. Dr. X. Shi designed the scope of this work and advised the team throughout the process (from conceptualization to manuscript preparation). The author(s) read and approved the final manuscript.

Funding

The authors thankfully acknowledge financial support by the USDOT (Tier 1 UTC CESTIC) and the NSF (Award No. 1638384).

Availability of data and materials

The datasets generated and/or analyzed during the current study are available in the Google Site repository, [<https://sites.google.com/site/greensmartinfrastructure/ApplePomaceInhibitorDatasets.zip>].

Competing interests

The authors declare no competing interest.

Author details

¹Department of Civil & Environmental Engineering, Laboratory of Corrosion Science and Electrochemical Engineering, National Center for Transportation Infrastructure & Life-Extension, Washington State University, P. O. Box 642910, Pullman, WA 99164-2910, USA. ²Department of Chemistry, College of Science, Al-Nahrain University, Baghdad 64021, Iraq.

Received: 12 August 2019 Accepted: 5 May 2020

Published online: 05 June 2020

References

1. Abd El-Lateef HM, Abu-Dief AM, Abdel-Rahman LH, Sañudo EC, Aliaga-Alcalde N (2015) Electrochemical and theoretical quantum approaches on the inhibition of C1018 carbon steel corrosion in acidic medium containing chloride using some newly synthesized phenolic Schiff bases compounds. *J Electroanal Chem* 743:120–133. <https://doi.org/10.1016/j.jelechem.2015.02.023>
2. Albright M (2005) Changes in water quality in an urban stream following the use of organically derived deicing products. *Lake Reserv Manag* 21:119–124. <https://doi.org/10.1080/07438140509354419>
3. Al-Fakih AM, Abdallah HH, Aziz M (2019) Experimental and theoretical studies of the inhibition performance of two furan derivatives on mild steel corrosion in acidic medium. *Mater Corros* 70:135–148. <https://doi.org/10.1002/maco.201810221>
4. Allen GC, Curtis MT, Hooper AJ, Tucker PM (1974) X-ray photoelectron spectroscopy of iron–oxygen systems. *J Chem Soc Dalton Trans*:1525–1530. <https://doi.org/10.1039/DT9740001525>
5. Allen GC, Hallam KR (1996) Characterisation of the spinels $MxCo_{1-x}Fe_2O_4$ ($M = Mn, Fe$ or Ni) using X-ray photoelectron spectroscopy. *Appl Surf Sci* 93:25–30. [https://doi.org/10.1016/0169-4332\(95\)00186-7](https://doi.org/10.1016/0169-4332(95)00186-7)
6. Aloysius A, Ramanathan R, Christy A, Baskaran S, Antony N (2017) Experimental and theoretical studies on the corrosion inhibition of vitamins – thiamine hydrochloride or biotin in corrosion of mild steel in aqueous chloride environment. *Egypt J Pet*. <https://doi.org/10.1016/j.ejpe.2017.06.003>
7. Appleman BR (1987) Painting over soluble salts: a perspective. *J Prot Coat Linings* 4:68–82
8. Ashassi-Sorkhabi H, Asghari E (2008) Effect of hydrodynamic conditions on the inhibition performance of L-methionine as a “green” inhibitor. *Electrochim Acta* 54:162–167. <https://doi.org/10.1016/j.electacta.2008.08.024>
9. Ashassi-Sorkhabi H, Seifzadeh D, Hosseini MG (2008) EN, EIS and polarization studies to evaluate the inhibition effect of 3H-phenothiazin-3-one, 7-dimethylamin on mild steel corrosion in 1 M HCl solution. *Corros Sci* 50: 3363–3370. <https://doi.org/10.1016/j.corsci.2008.09.022>
10. Behpour M, Ghoreishi SM, Khayatkhani M, Soltani N (2012) Green approach to corrosion inhibition of mild steel in two acidic solutions by the extract of Punica granatum peel and main constituents. *Mater Chem Phys* 131:621–633. <https://doi.org/10.1016/j.matchemphys.2011.10.027>
11. Bin Ibrahim MF (2013) Effect of different sodium chloride (NaCl) concentration on corrosion of coated steel (bachelor of mechanical engineering). Universiti Malaysia Pahang. Pahang, Malaysia
12. Bommersbach P, Alemany-Dumont C, Millet JP, Normand B (2005) Formation and behaviour study of an environment-friendly corrosion inhibitor by electrochemical methods. *Electrochim Acta* 51:1076–1084. <https://doi.org/10.1016/j.electacta.2005.06.001>
13. Bozorg M, Shahrabi Farahani T, Neshati J, Chaghazardi Z, Mohammadi Ziarani G (2014) Myrtus Communis as green inhibitor of copper corrosion in sulfuric acid. *Ind Eng Chem Res* 53:4295–4303. <https://doi.org/10.1021/ie404056w>
14. Cao C (1996) On electrochemical techniques for interface inhibitor research. *Corros Sci* 38:2073–2082. [https://doi.org/10.1016/S0010-938X\(96\)00034-0](https://doi.org/10.1016/S0010-938X(96)00034-0)
15. Chen Y, Xing W, Wang L, Chen L (2019) Experimental and electrochemical research of an efficient corrosion and scale inhibitor. *Mater Basel Switz* 12. <https://doi.org/10.3390/ma12111821>
16. Cheng KC, Guthrie TF (1998) Liquid road deicing environment impact (498–0670). Insurance Corporation of British Columbia. North Vancouver
17. Chevalier M, Robert F, Amusan N, Traisnel M, Roos C, Lebrini M (2014) Enhanced corrosion resistance of mild steel in 1M hydrochloric acid solution by alkaloids extract from Aniba rosaeodora plant: electrochemical, phytochemical and XPS studies. *Electrochimica Acta, Electrochem Impedance Spectroscopy* 131:96–105. <https://doi.org/10.1016/j.electacta.2013.12.023>
18. Chigondo M, Chigondo F (2016) Recent natural corrosion inhibitors for mild steel: an overview. *J Chem* 2016:1–7. <https://doi.org/10.1155/2016/6208937>
19. Dariva CG, Galio AF, 2014. Corrosion inhibitors – principles, mechanisms and applications, in: Aliofkhaezai, M. (Ed.), Developments in corrosion protection. InTechOpen, London
20. Dong S, Yuan X, Chen S, Zhang L, Huang T (2018) A novel HPEI-based Hyperbranched scale and corrosion inhibitor: construction, performance, and inhibition mechanism. *Ind Eng Chem Res* 57:13952–13961. <https://doi.org/10.1021/acs.iecr.8b03522>
21. Ebadi M, Basirun WJ, Khaledi H, Ali HM (2012) Corrosion inhibition properties of pyrazolylindolenine compounds on copper surface in acidic media. *Chem Cent J* 6:163. <https://doi.org/10.1186/1752-153X-6-163>
22. Ebenso EE, Kabanda MM, Murulana LC, Singh AK, Shukla SK (2012) Electrochemical and quantum chemical investigation of some Azine and thiazine dyes as potential corrosion inhibitors for mild steel in hydrochloric acid solution. *Ind Eng Chem Res* 51:12940–12958. <https://doi.org/10.1021/ie300965k>
23. El-Hafez GMA, Badawy WA (2013) The use of cysteine, N-acetyl cysteine and methionine as environmentally friendly corrosion inhibitors for Cu–10Al–5Ni alloy in neutral chloride solutions. *Electrochim Acta* 108:860–866. <https://doi.org/10.1016/j.electacta.2013.06.079>
24. Fay L, Nazari MH, Jungwirth S, Muthumani A (2015) Snow and ice control environmental best management practices. *Environ Sustain Transp Infrastruct, Proc*:147–161. <https://doi.org/10.1061/9780784479285.013>
25. Fernandes PAR, Ferreira SS, Bastos R, Ferreira I, Cruz MT, Pinto A, Coelho E, Passos CP, Coimbra MA, Cardoso SM, Wessel DF (2019) Apple pomace extract as a sustainable food ingredient. *Antioxidants* 8. <https://doi.org/10.3390/antiox8060189>
26. Fouda AS, Megahed HE, Fouad N, Elbahravi NM (2016) Corrosion inhibition of carbon steel in 1 M hydrochloric acid solution by aqueous extract of Thevetia peruviana. *J Bio- Tribo-Corros* 2:1–13. <https://doi.org/10.1007/s40735-016-0046-z>
27. Frear C, Zhao B, Fu G, Richardson M, Chen S, Fuchs MR (2005) Biomass inventory and bioenergy assessment (final report no. 05–07–047). Washington State Department of Ecology. Olympia
28. Gabrielli C, Huet F, Keddam M, Oltra R (1990) A review of the probabilistic aspects of localized corrosion. *CORROSION* 46:266–278. <https://doi.org/10.5006/1.3585102>
29. Honarvar Nazari M, Havens EA, Muthumani A, Shi X (2019) Effects of processed agro-residues on the performance of sodium chloride brine anti-icer. *ACS Sustain Chem Eng* 7:13655–13667. <https://doi.org/10.1021/acsschemeng.8b06043>
30. Honarvar Nazari M, Laura F, Jungwirth S, Shi X (2015) Water quality implications and the toxicological effects of chloride-based deicers. *Environ Sustain Transp Infrastruct, proceedings*:272–292. <https://doi.org/10.1061/9780784479285.022>
31. Honarvar Nazari M, Xianming S (2019) Developing renewable agro-based anti-icers for sustainable winter road maintenance operations. *J Mater Civ Eng* 31:04019299. [https://doi.org/10.1061/\(ASCE\)MT.1943-5533.0002963](https://doi.org/10.1061/(ASCE)MT.1943-5533.0002963)
32. Hong T, Shi H, Wang H, Gopal M, Jepson WP (2000) EIS study of corrosion product film in pipelines. *CORROSION2000*. Presented at the CORROSION2000, NACE International, Orlando, p 16
33. Hsu C, Nazari MH, Li Q, Shi X (2019) Enhancing degradation and corrosion resistance of AZ31 magnesium alloy through hydrophobic coating. *Mater Chem Phys*. <https://doi.org/10.1016/j.matchemphys.2018.12.106>
34. Hunter T (2012) Why nature chose phosphate to modify proteins. *Philos Trans R Soc B Biol Sci* 367:2513–2516. <https://doi.org/10.1098/rstb.2012.0013>

35. Husain A, Kupwade-Patil K, Al-Aibani AF, Abdulsalam MF (2017) In situ electrochemical impedance characterization of cement paste with volcanic ash to examine early stage of hydration. *Construct Build Mater* 133:107–117. <https://doi.org/10.1016/j.conbuildmat.2016.12.054>
36. Jamil HE, Shiri A, Boulif R, Bastos C, Montemor MF, Ferreira MGS (2004) Electrochemical behaviour of amino alcohol-based inhibitors used to control corrosion of reinforcing steel. *Electrochim Acta* 49:2753–2760. <https://doi.org/10.1016/j.electacta.2004.01.041>
37. Jianlin W, Hui Y, Xianming S (2016) Effectiveness of products in managing metallic corrosion induced by cyclic deicer exposure: laboratory study using multielectrode Array sensors, electrochemical impedance, and laser Profilometer. *J Mater Civ Eng* 28:04015186. [https://doi.org/10.1061/\(ASCE\)MT.1943-5533.0001449](https://doi.org/10.1061/(ASCE)MT.1943-5533.0001449)
38. Kamal C, Sethuraman MG (2012) Caulerpin—a bis-indole alkaloid as a green inhibitor for the corrosion of mild steel in 1 M HCl solution from the marine alga *Caulerpa racemosa*. *Ind Eng Chem Res* 51:10399–10407. <https://doi.org/10.1021/ie3010379>
39. Kim Y-S, Kim J-G (2017) Corrosion behavior of pipeline carbon steel under different iron oxide deposits in the district heating system. *Metals* 7:182. <https://doi.org/10.3390/met7050182>
40. Liu Y, Zou C, Yan X, Xiao R, Wang T, Li M (2015) β -Cyclodextrin modified natural chitosan as a green inhibitor for carbon steel in acid solutions. *Ind Eng Chem Res* 54:5664–5672. <https://doi.org/10.1021/acs.iecr.5b00930>
41. Lobo MG, Dorta E (2019) Chapter 19 - utilization and Management of Horticultural Waste. In: Yahia EM (ed) *Postharvest Technology of Perishable Horticultural Commodities*. Woodhead publishing, pp 639–666. <https://doi.org/10.1016/B978-0-12-813276-0.00019-5>
42. Luo J, Xu Y, Fan Y (2019) Upgrading pectin production from apple pomace by acetic acid extraction. *Appl Biochem Biotechnol* 187:1300–1311. <https://doi.org/10.1007/s12010-018-2893-1>
43. Ma F-Y (2012) Corrosive effects of chlorides on metals. *Pitting Corros*. <https://doi.org/10.5772/32333>
44. Ma H, Cheng X, Li G, Chen S, Quan Z, Zhao S, Niu L (2000) The influence of hydrogen sulfide on corrosion of iron under different conditions. *Corros Sci* 42:1669–1683. [https://doi.org/10.1016/S0010-938X\(00\)00003-2](https://doi.org/10.1016/S0010-938X(00)00003-2)
45. Markin VS, Volkova-Gugeshashvili MI, Volkov AG (2006) Adsorption at liquid interfaces: the generalized Langmuir isotherm and interfacial structure. *J Phys Chem B* 110:11415–11420. <https://doi.org/10.1021/jp061818v>
46. McIntyre NS, Zetaruk DG (1977) X-ray photoelectron spectroscopic studies of iron oxides. *Anal Chem* 49:1521–1529. <https://doi.org/10.1021/ac50019a016>
47. Mei L, Liao L, Wang Z, Xu C (2015) Interactions between phosphoric/tannic acid and different forms of FeOOH. *Adv Mater Sci Eng* 10. <https://doi.org/10.1155/2015/250836>
48. Musa AY, Kadhum AAH, Mohamad AB, Rahoma AAB, Mesmari H (2010) Electrochemical and quantum chemical calculations on 4,4-dimethylloxazolidine-2-thione as inhibitor for mild steel corrosion in hydrochloric acid. *J Mol Struct* 969:233–237. <https://doi.org/10.1016/j.molstruc.2010.02.051>
49. Nazari MH, Allahkaram SR (2010) The effect of acetic acid on the CO₂ corrosion of grade X70 steel. *Mater Des* 31:4290–4295. <https://doi.org/10.1016/j.matdes.2010.04.002>
50. Nazari MH, Shi X (2018) Vehicle risks of winter road operations and best management practices. In: *Sustainable winter road operations*. Wiley-Blackwell, pp 241–272. <https://doi.org/10.1002/9781119185161.ch12>
51. Nazari MH, Shihab MS, Cao L, Havens EA, Shi X (2017) A peony-leaves-derived liquid corrosion inhibitor: protecting carbon steel from NaCl. *Green Chem Lett Rev* 10:359–379. <https://doi.org/10.1080/17518253.2017.1388446>
52. Negm NA, Elkholy YM, Zahran MK, Tawfik SM (2010) Corrosion inhibition efficiency and surface activity of benzothiazol-3-ium cationic Schiff base derivatives in hydrochloric acid. *Corros Sci* 52:3523–3536. <https://doi.org/10.1016/j.corsci.2010.07.001>
53. Nixon WA, Williams AD (2001) A guide for selecting anti-icing chemicals, Version 1.0 (IIHR Technical Report No. No. 420)
54. Nwabanne JT, Okafor VN (2012) Adsorption and thermodynamics study of the inhibition of corrosion of mild steel in H₂SO₄ medium using *Vernonia amygdalina*. *J Miner Mater Charact Eng* 11:885–890
55. Obot IB, Gasem ZM (2014) Theoretical evaluation of corrosion inhibition performance of some pyrazine derivatives. *Corros Sci* 83:359–366. <https://doi.org/10.1016/j.corsci.2014.03.008>
56. Obot IB, Obi-Egbedi NO (2010) Theoretical study of benzimidazole and its derivatives and their potential activity as corrosion inhibitors. *Corros Sci* 52: 657–660. <https://doi.org/10.1016/j.corsci.2009.10.017>
57. Oguzie EE (2007) Corrosion inhibition of aluminium in acidic and alkaline media by *Sansevieria trifasciata* extract. *Corros Sci* 49:1527–1539. <https://doi.org/10.1016/j.corsci.2006.08.009>
58. Osman MM, Omar AMA, Al-Sabagh AM (1997) Corrosion inhibition of benzyl triethanol ammonium chloride and its ethoxylate on steel in sulphuric acid solution. *Mater Chem Phys* 50:271–274. [https://doi.org/10.1016/S0254-0584\(97\)01941-X](https://doi.org/10.1016/S0254-0584(97)01941-X)
59. Pandarinathan V, Lepková K, Bailey SI, Becker T, Gubner R (2014) Adsorption of corrosion inhibitor 1-Dodecylpyridinium chloride on carbon steel studied by in situ AFM and electrochemical methods. *Ind Eng Chem Res* 53:5858–5865. <https://doi.org/10.1021/ie402784y>
60. Paparazzo E (1987) XPS and auger spectroscopy studies on mixtures of the oxides SiO₂, Al₂O₃, Fe₂O₃ and Cr₂O₃. *J Electron Spectrosc Relat Phenom* 43:97–112. [https://doi.org/10.1016/0368-2048\(87\)80022-1](https://doi.org/10.1016/0368-2048(87)80022-1)
61. Pelavin M, Hendrickson DN, Hollander JM, Jolly WL (1970) Phosphorus 2p electron binding energies. Correlation with extended Hückel charges. *J Phys Chem* 74:1116–1121. <https://doi.org/10.1021/j100700a027>
62. Pradityana A, Sulistijono SA, Chyntara S (2014) Eco-friendly green inhibitor of mild steel in 3.5% NaCl solution by Sarang Semut (*Myrmecodia Pendants*) extract. *AIP Conf Proc* 1617:161–164. <https://doi.org/10.1063/1.4897128>
63. Pradityana A, Sulistijono SA, Noerachim L, Susanti D (2016) Inhibition of corrosion of carbon steel in 3.5% NaCl solution by *Myrmecodia Pendants* extract. *Int J Corros* 6. <https://doi.org/10.1155/2016/6058286>
64. Rani BEA, Basu BBJ (2012) Green inhibitors for corrosion protection of metals and alloys: an overview [WWW document]. *Int J Corros*. <https://doi.org/10.1155/2012/380217>
65. Recloux I, Andreatta F, Druart M-E, Coelho LB, Cepek C, Cossement D, Fedrizzi L, Olivier M-G (2018) Stability of benzotriazole-based films against AA2024 aluminium alloy corrosion process in neutral chloride electrolyte. *J Alloys Compd* 735:2512–2522. <https://doi.org/10.1016/j.jallcom.2017.11.346>
66. Ryl J, Brodowski M, Kowalski M, Lipinska W, Niedzialkowski P, Wysocka J (2019) Corrosion inhibition mechanism and efficiency differentiation of Dihydroxybenzene isomers towards aluminum alloy 5754 in alkaline media. *Materials* 12. <https://doi.org/10.3390/ma12193067>
67. Sahu O, Singh N (2019) 13 - significance of bioadsorption process on textile industry wastewater. In: Shahid-ul-Islam BBS (ed) *The impact and prospects of green chemistry for textile technology*, The textile institute book series. Woodhead publishing, pp 367–416. <https://doi.org/10.1016/B978-0-08-102491-1.00013-7>
68. Shah AM, Rahim AA, Hamid SA, Yahya S (2013) Green inhibitors for copper corrosion by mangrove tannin. *Int J Electrochem Sci* 8:2140–2153
69. Shi X, Fay L, Yang Z, Nguyen TA, Liu Y (2009) Corrosion of deicers to metals in transportation infrastructure: introduction and recent developments. *Corrosion Rev* 27:23–52. <https://doi.org/10.1515/CORRREV.2009.27.1-2.23>
70. Shihab MS, Mahmood AF (2017) Experimental and theoretical study of some Npyridinium salt derivatives as corrosion inhibitors for mild-steel in 1 M H₂SO₄. *Port. Electrochim Acta* 35:39–51. <https://doi.org/10.4152/pea.201701039>
71. Shihab MS, Nazari MH, Fay L (2016) Study of inhibition effect of pyridinium salt derivative on corrosion of C1010 carbon steel in saline solution. *Prot Met Phys Chem Surf* 52:714–720. <https://doi.org/10.1134/S2020205116040213>
72. Sin HLY, Abdul Rahim A, Gan CY, Saad B, Salleh MI, Umeda M (2017) *Aquilaria subintergra* leaves extracts as sustainable mild steel corrosion inhibitors in HCl. *Measurement* 109:334–345. <https://doi.org/10.1016/j.measurement.2017.05.045>
73. Somasundaran P (2004) *Encyclopedia of surface and colloid science*, 2004 update supplement. CRC Press. Boca Raton, FL, USA
74. Stewart JJP (1989) Optimization of parameters for semiempirical methods I. *Method J Comput Chem* 10:209–220. <https://doi.org/10.1002/jcc.540100208>
75. Suarez R, Gonzalez-Rodriguez J, Dominguez-Patino G, Martinez-Villafane A (2014) Use of *Opuntia ficus* extract as a corrosion inhibitor for carbon steel in acidic media. *Anti-Corros Methods Mater* 61. <https://doi.org/10.1108/ACMM-01-2013-1238>
76. Suedile F, Robert F, Roos C, Lebrini M (2014) Corrosion inhibition of zinc by *Mansoa alliacea* plant extract in sodium chloride media: extraction, characterization and electrochemical studies. *Electrochim Acta* 133:631–638. <https://doi.org/10.1016/j.electacta.2013.12.070>

77. Surendranath Y, Kanan MW, Nocera DG (2010) Mechanistic studies of the oxygen evolution reaction by a cobalt-phosphate catalyst at neutral pH. *J Am Chem Soc* 132:16501–16509. <https://doi.org/10.1021/ja106102b>
78. Tao Z, He W, Wang S, Zhou G (2013) Electrochemical study of Cyproconazole as a novel corrosion inhibitor for copper in acidic solution. *Ind Eng Chem Res* 52:17891–17899. <https://doi.org/10.1021/ie402693d>
79. Umoren SA, Obot IB, Madhankumar A, Gasem ZM (2015) Performance evaluation of pectin as ecofriendly corrosion inhibitor for X60 pipeline steel in acid medium: experimental and theoretical approaches. *Carbohydr Polym* 124:280–291. <https://doi.org/10.1016/j.carbpol.2015.02.036>
80. Verma C, Quraishi MA, Kluza K, Makowska-Janusik M, Olasunkanmi LO, Ebenso EE (2017) Corrosion inhibition of mild steel in 1M HCl by D-glucose derivatives of dihydropyrido [2,3-d:6,5-d'] dipyrimidine-2, 4, 6, 8(1H,3H, 5H,7H)-tetraone. *Sci Rep* 7:44432. <https://doi.org/10.1038/srep44432>
81. Wang X, Chen Q, Lü X (2014) Pectin extracted from apple pomace and citrus peel by subcritical water. *Food Hydrocoll* 38:129–137. <https://doi.org/10.1016/j.foodhyd.2013.12.003>
82. Yoshida T, Sawada S (1974) X-ray photoelectron spectroscopy of EDTA. *Bull Chem Soc Jpn* 47:50–53. <https://doi.org/10.1246/bcsj.47.50>
83. Zhang Y, Tian J, Zhong J, Shi X (2018) Thin nacre-biomimetic coating with super-anticorrosion performance. *ACS Nano* 12:10189–10200. <https://doi.org/10.1021/acsnano.8b05183>

Publisher's Note

Springer Nature remains neutral with regard to jurisdictional claims in published maps and institutional affiliations.

Submit your manuscript to a SpringerOpen[®] journal and benefit from:

- Convenient online submission
- Rigorous peer review
- Open access: articles freely available online
- High visibility within the field
- Retaining the copyright to your article

Submit your next manuscript at ► [springeropen.com](https://www.springeropen.com)